Available online at website: https://journal.bcrec.id/index.php/bcrec

Bulletin of Chemical Reaction Engineering & Catalysis, 19 (3) 2024, 372-383

Research Article

Exploring Alkali Hydroxide Influence on Calcium Titanate Formation for Application in Biodiesel Catalysts

Ratchadaporn Puntharod*, Kittikarnkorn Onsomsuay, Pusit Pookmanee, Jaturon Kumchompoo

Department of Chemistry, Faculty of Science, Maejo University, Chiang Mai, 50290, Thailand.

Received: 12th June 2024; Revised: 18th July 2024; Accepted: 19th July 2024
Available online: 22th July 2024; Published regularly: October 2024

Abstract

Biodiesel has been recognized as the most widely utilized biofuel around the world due to its significant role in reducing the consumption of crude oil and lowering environmental pollution levels. By serving as a renewable alternative to fossil fuels, bioethanol helps decrease greenhouse gas emissions and contributes to a more sustainable energy future. Traditionally, alkali hydroxides like NaOH and KOH have been mainstays in biodiesel synthesis. However, their overuse can lead to unwanted byproducts and operational complexities. Since calcium titanate can occur at a strong base condition, it presents an alternative avenue worth exploring. In this study, we investigate the influence of alkali hydroxides, namely LiOH, NaOH, and KOH, on the formation of calcium titanate through hydrothermal methods, with varying heating times. We aim to understand how different hydroxides affect the synthesis process and the resultant properties of calcium titanate. We delve into the vibrational properties of Ca–O–Ti and Ti–O bonds using Fourier Transform Infra Red (FTIR) spectroscopy, confirming the presence of calcium titanate (JCPDS No.42-0423) through X-ray Diffractometry (XRD). This thorough characterization provides insight into the structural integrity and composition of the synthesized materials. Moreover, Scanning Electron Microscopy (SEM) reveals the intriguing cube-like morphology of calcium titanate, offering visual evidence of its unique structure. The fatty acid methyl ester impressively-show that calcium titanate synthesized in 7 M NaOH and KOH solutions, heated for 24 h, emerges as a promising biodiesel catalyst. We observe fatty acid methyl ester provides the percentages of 63.67% and 90.02%, respectively, indicating the catalytic efficacy of these materials in biodiesel production. These findings not only contribute to the understanding of calcium titanate synthesis but also pave the way for a sustainable future in biodiesel production by introducing efficient and eco-friendly catalysts.

Copyright © 2024 by Authors, Published by BCREC Publishing Group. This is an open access article under the CC BY-SA License (https://creativecommons.org/licenses/by-sa/4.0).

Keywords: $CaTiO_3$; alkali hydroxide; biodiesel catalyst; transesterification; hydrothermal

How to Cite: R. Puntharod, K. Onsomsuay, P. Pookmanee, J. Kumchompoo (2024). Exploring Alkali Hydroxide Influence on Calcium Titanate Formation for Application in Biodiesel Catalysts. *Bulletin of Chemical Reaction Engineering & Catalysis*, 19 (3), 372-383 (doi: 10.9767/bcrec.20165)

Permalink/DOI: https://doi.org/10.9767/bcrec.20165

1. Introduction

Titanate-based materials have found widespread application across various domains. For instance, titanate nanotubes have been utilized in photocatalytic water decontamination [1], while calcium copper titanates ($CaCu_3Ti_4O_{12}$) serve in resonators, capacitors, and sensors [2]. The spinel lithium titanate ($Li_4Ti_5O_{12}$) has garnered attention for its role in energy storage devices [3], and the emergence of ferroelectric properties in $ATiO_3$ compounds (where A = Ca, Sr, Ba) has been investigated [4]. A particularly intriguing application of titanate complexes lies in biodiesel catalysis. Nanotubular sodium titanate ($Na_2Ti_3O_7.nH_2O$) has demonstrated remarkable efficiency, yielding up to 100% biodiesel [5]. Likewise, strontium titanate perovskite has shown promise as a heterogeneous catalyst, with reusability observed for up to six cycles and a 79% yield of fatty acid methyl ester [6]. Additionally, sodium titanate variants ($Na_2Ti_3O_7$ and

* Corresponding Author.
Email: ratchadaporn_p@mju.ac.th (R. Puntharod);
Telp: +66-53-873850-1. Fax: +66-53-873950

$Na_2Ti_6O_{13}$) have been utilized in the conversion of vegetable oil to biodiesel [7]. The advantages of $CaTiO_3$ likely include its catalytic activity and selectivity in the transesterification reaction for biodiesel production. Using a factorial design allows researchers to systematically vary synthesis parameters and optimize the catalyst's properties. $CaTiO_3$ may offer advantages such as high stability, efficiency in converting triglycerides to biodiesel, and potentially lower cost compared to other catalysts.

Calcium titanate ($CaTiO_3$), characterized by its perovskite structure, has emerged as a versatile material with wide-ranging applications. It serves as an electrode material for electrochemical urea sensing [8] and demonstrates efficacy in the photocatalytic degradation of methylene blue, as well as in biodiesel catalysis [9]. In the biodiesel production landscape, alkali hydroxides, like NaOH and KOH, are commonly employed as homogeneous catalysts, albeit with the drawback of necessitating additional steps and expenses for neutralization [10,11]. Heterogeneous catalysts present an attractive alternative, promising cost reduction and yields exceeding 90% [12].

Among the various alternative fuels that are available, those derived from naturally harmless vegetables emerge as the most preferable and advantageous option, due to their potential to serve as an effective and sustainable energy source. In particular, waste cooking oil stands out as a remarkably promising and viable candidate for contributing to the enhancement of sustainability efforts, the improvement of energy efficiency, and, perhaps most crucially, the preservation of energy resources for future generations. This is because, when repurposed, waste cooking oil can be transformed into a renewable energy source that not only helps to reduce environmental impact but also supports long-term energy conservation goals. Herein lies the appeal of $CaTiO_3$ as a biodiesel catalyst. Utilized in transesterification reactions, $CaTiO_3$ offers distinct advantages, notably its facile separation from the reactants, enhancing process efficiency and scalability. Synthesizing calcium titanate as a heterogeneous biodiesel catalyst offers a spectrum of methods, each tailored to specific reactants and applications. Green synthesis, utilizing leaf extracts [13], alongside techniques like sol-gel-hydrothermal synthesis [14], solid-state reaction [15], and spray pyrolysis [16], exemplify the diverse approaches available.

The choice of synthesis method hinges upon various factors. Notably, the influence of alkali hydroxides, comprising alkali metals and hydroxide ions, cannot be overlooked [17,18]. Dong *et al*. [19] elucidated the pivotal role of sodium hydroxide in calcium titanate formation, as its occurrence is favored under strong base conditions. For instance, Dong *et al*. [20] demonstrated the solvothermal synthesis of calcium titanate at 180 °C, employing calcium chloride dihydrate and titanium tetrabutoxide as precursors, with pH adjustment to 12 using 7 M sodium hydroxide [20].

In 2020, our research group successfully synthesized silicate compounds from LiOH and KOH to produce lithium silicate (Li_2SiO_3) and potassium silicate (K_2SiO_3) using the hydrothermal microwave method. These silicates can serve as heterogeneous biodiesel catalysts. The results indicate that K_2SiO_3 represents the optimal alkali silicate for achieving a high weight percentage of fatty acid methyl esters (FAME), approximately 88.40% [21]. In this research, we investigated the effects of various alkali hydroxides on the synthesis of $CaTiO_3$. The research delved into the impact of alkali hydroxides lithium hydroxide, sodium hydroxide, and potassium hydroxide on the formation of calcium titanate. Utilizing calcium carbonate and titanium dioxide as precursors, calcium titanate synthesis via the hydrothermal method was chosen for its ability to yield highly crystalline products. Characterization of the synthesized materials was conducted using Fourier transform infrared spectroscopy, scanning electron microscopy, and X-ray diffractometry. Subsequently, the synthesized calcium titanate was evaluated for its catalytic efficacy in the transesterification reaction for biodiesel production.

2. Materials and Methods

2.1 Preparation of Calcium Titanate

The experiment involved dissolving 3.00 g of calcium carbonate ($CaCO_3$, Unilab, 97.55%) and 2.40 g of titanium dioxide (TiO_2, Loba, 98%) in 3 ml of concentrated nitric acid (HNO_3, RCI Labscan 65%) each. Both solutions were heated and stirred with a magnetic bar until homogeneous. Subsequently, the calcium carbonate solution was slowly added dropwise to the titanium dioxide solution. The resulting mixture was then adjusted to a volume of 12 mL using deionized water and heated further. Following this, each solution was gradually mixed with 15 mL of 7 M lithium hydroxide (LiOH, Fisher Chemical, 100%), sodium hydroxide (NaOH, Fisher Chemical, 97%), and potassium hydroxide (KOH, Qrec, 85%). The resulting mixture was transferred to a Teflon tube and heated at 180 °C in a hot air oven for 18 and 24 h.

The filtered product was then heated at 90 °C for 6 h. Finally, the solid product was characterized using Fourier transform infrared spectroscopy, scanning electron microscopy, and

Copyright © 2024, ISSN 1978-2993

X-ray diffractometry. The fatty acid methyl ester (FAME) represents the efficiency and effectiveness of biodiesel production. The free fatty acid methyl ester was carried out by gas chromatography-mass spectrometry with standard carbon C17.

2.2 Characterization of Calcium Titanate

The solid products were characterized by Fourier transform infrared spectroscopy (FTIR), scanning electron microscopy (SEM), and X-ray diffractometry (XRD). FTIR: The infrared spectra were measured on Perkin Elmer model Spectrum RXI with KBr preparation. The spectra were collected over the range of wavenumber 4,000-400 cm^{-1} with 16 scanning and resolution at 4 cm^{-1}. SEM: The morphology and aggregate of particles were examined by JEOL model JEM-6335. XRD: The structures of samples were identified by using Cu-Kα radiation and XRD pattern on Philips model X'Pert MPD.

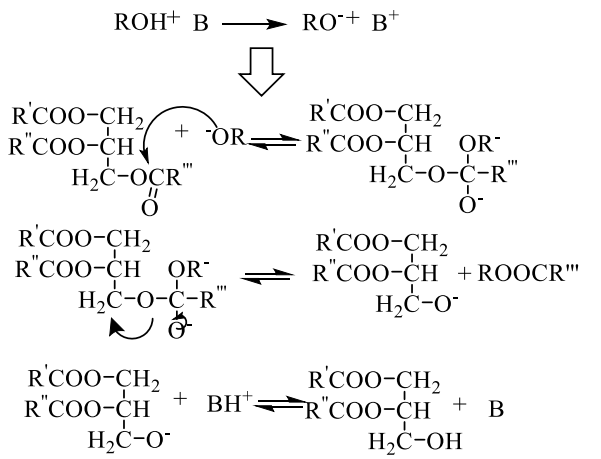

B = base from $CaTiO_3$ under various alkali hydroxide

Scheme 1. Reaction mechanism of trans-esterification reaction.

2.3 Transesterification Reaction of Biodiesel

The 100 mL of palm oil was mixed with 25 mL of methanol in a round bottom bottle with reflux apparatus for a transesterification reaction (Scheme 1). The 1.5 g of calcium titanate was added and heated to the mixture at 60-70 °C for 3 h. The mixture was poured into the separating funnel and let stand until the separation appeared then the mixture was filtrated. The warm water was added to the oil fraction in a ratio of 1:1 volume by volume and was stirred for 30 min.

The methyl ester in biodiesel was determined by gas chromatography (Agilent model 7890A) with HP-5 MS 0.25 mm × 30 m × 0.25 µm. The carrier gas was helium. The inlet temperature was 230 °C with column flow was 1.5 mL/min. The injector type was splitless and injection volume was 1.0 µL. The split ratio was 50:1. The standard of fatty acid methyl ester was used C17 (Sigma

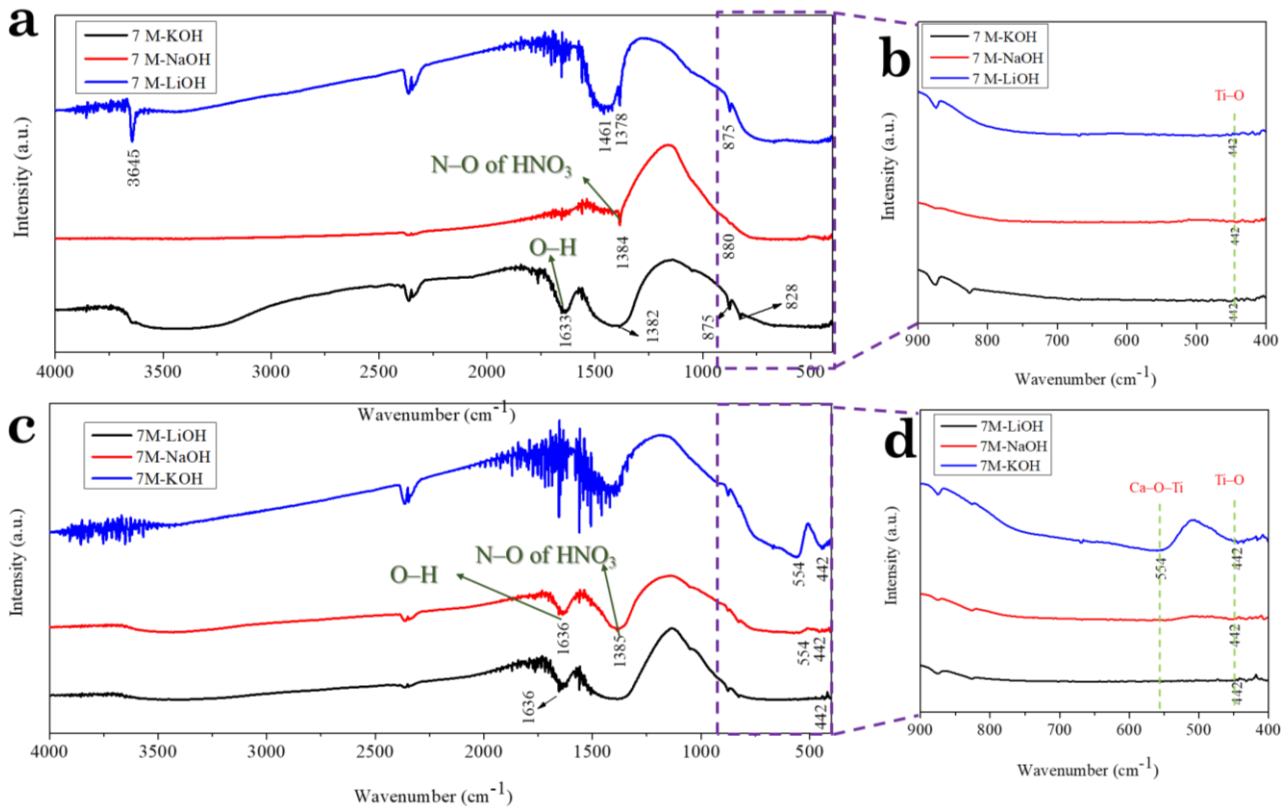

Figure 1. FTIR spectra of products synthesized in the condition of 7 M (a) LiOH, NaOH, and KOH at 180 °C for 18 h and (b) LiOH, NaOH and KOH at 180 °C for 24 h.

Copyright © 2024, ISSN 1978-2993

Aldrich). The viscosity at 40 °C was measured by capillary (Cannon) with a constant equal to 0.958 cSt/s.

The yield of biodiesel from palm oil was determined by Equation (1) [22,23].

$$Yield\ of\ biodiesel = \frac{weight\ of\ biodiesel}{weight\ of\ palm\ oil} \times 100 \quad (1)$$

The percentage of fatty acid methyl ester was calculated in Equation (2) [24].

$$C = \frac{\left(\sum A\right) - A_{EI}}{A_{EI}} \times \frac{C_{EI} \times V_{EI}}{m} \times 100\% \quad (2)$$

Where, C is %FAME, A is area peak of C16-C24, A_{EI} is area peak of C17 methyl ester, C_{EI} is area peak of C17 methyl ester(mg/mL), V_{EI} is volume of C17 methyl ester, and m is weight of biodiesel (mg).

3. Results and Discussion

3.1. Characterizations of $CaTiO_3$

The vibration of the metal-ligand mode was studied using Fourier transform infrared spectroscopy (FTIR). Figure 1(a) depicts the FTIR spectra results of the 7 M alkali hydroxide solutions at 180 °C for 18 h. The vibrations of the Ti–O bond and Ca–O–Ti were not clear due to broad bands. To enable a more detailed and focused observation of the magnified spectral data, we will specifically direct our attention to the Ti–O vibrational band region at approximately 442 cm^{-1}, as illustrated in Figure 1(b). In this detailed spectral analysis, we note that the Ti–O vibrational mode of the $CaTiO_3$ sample, which was synthesized using the 18 h hydrothermal method, is characterized by a broad peak. This broad peak is indicative of the presence of excess moisture contamination, which is further corroborated by the observation of an additional prominent peak located around 3500 cm^{-1}. This peak at 3500 cm^{-1} can be attributed to the vibrational modes associated with water molecules, reflecting the residual moisture in the sample and highlighting the need for meticulous control of experimental conditions to mitigate such contamination effects.

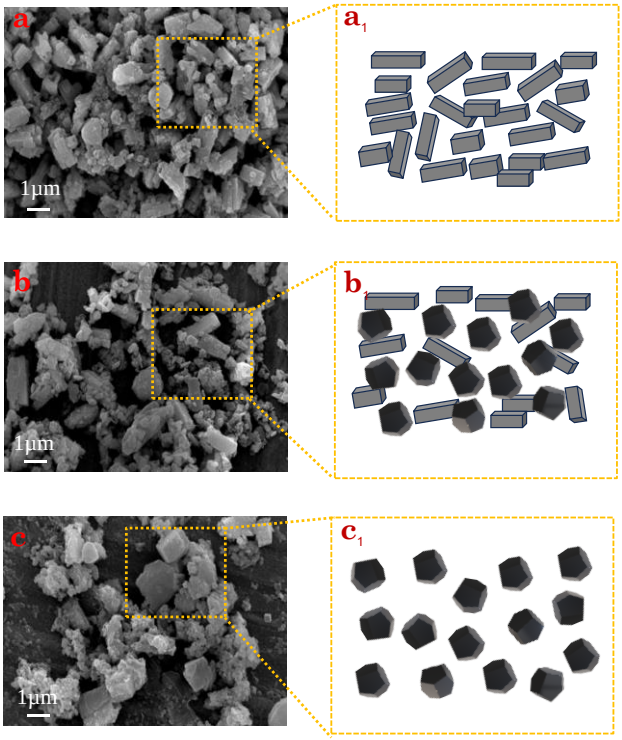

Figure 2. The product morphology was synthesized in (a) 7 M LiOH (b) 7 M NaOH and (c) 7 M KOH at 180 °C for 18 h and schematics of morphology shapes from (a1) 7 M LiOH (b1) 7 M NaOH and (c1) KOH.

In Figure 1(c), when the heating time was extended to 24 h, the Ti–O stretching band occurred at 454 and 444 cm^{-1} in 7 M NaOH and KOH, respectively. The bands at 556 and 551 cm^{-1} were assigned to the Ti–O–Ti bridge stretching in 7 M LiOH and NaOH, respectively. Additionally, bands at 1635 and 1636 cm^{-1} were attributed to O–H bands in hydroxyls and water surfaces on the $CaTiO_3$ [25]. All conditions exhibited a band at 1385 cm^{-1}, assigned to N–O stretching of HNO_3 [26], which was used as the solution to dissolve $CaCO_3$ and TiO_2, the starting materials. The stretching and bending of the Ca–O–Ti bond in calcium titanate appeared under 7 M KOH at 564 cm^{-1} [27]. To gain a deeper understanding of the effects of hydrothermal treatment time on the vibrational characteristics of the synthesized materials, a detailed analysis of the magnified FTIR spectra will be conducted. Specifically focusing on the vibrational range from 900 to 400 cm^{-1} as shown in Figure 1(d). Within this spectral range, we will examine the intensity and characteristics of the vibrational modes associated with the Ca–Ti–O and Ti–O bonds. Notably, for samples treated with KOH as the base during the 24 h hydrothermal process, we observe the presence of strong and distinct absorption bands at 554 cm^{-1} and 442 cm^{-1}, which are indicative of the characteristic vibrational modes of Ca–Ti–O. In contrast, when using LiOH and NaOH as the base under identical hydrothermal conditions, the spectra reveal broad and overlapping bands corresponding to two different types of vibrational modes. This observation suggests that KOH is particularly effective in promoting the formation of $CaTiO_3$ during a 24 h hydrothermal treatment, whereas LiOH and NaOH do not achieve the same degree of specificity in generating these vibrational features, highlighting KOH superior

Copyright © 2024, ISSN 1978-2993

role in inducing the formation of $CaTiO_3$ under the studied conditions.

The morphology study, conducted using scanning electron microscopy (SEM), depicted the products synthesized under 7 M alkali hydroxide at 180 °C for 18 h. In Figure 2(a), rectangular bars with various sizes and crystal shapes are observed, while the corresponding schematic is shown in Figure 2(a_1). Figure 3(b) exhibits a coherent shape, resembling a mixture of spherical and rectangular structures, with the morphology scheme represented in Figure 2(b_1). In Figure 3(c), the products are predominantly grouped in a round shape with a cube-like appearance. Furthermore, to gain a deeper understanding of the morphology of all samples, the morphology graphics are depicted in Figure 2(c_1).

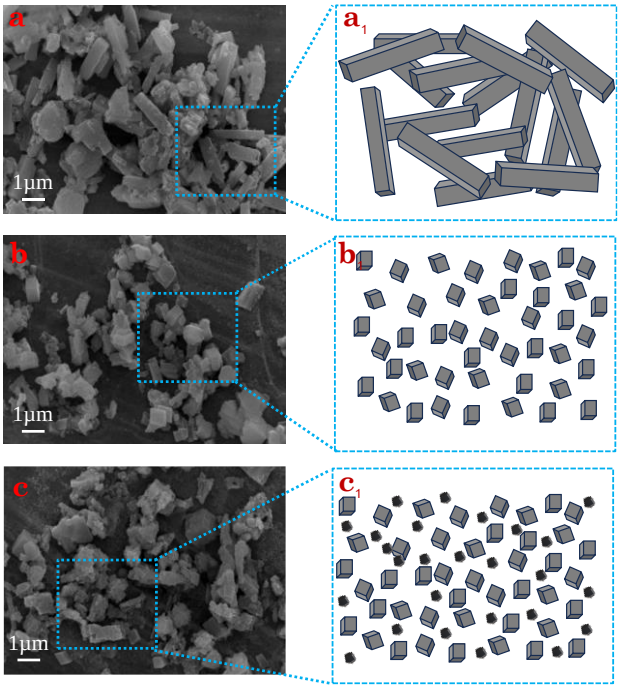

Figure 3. The product morphology was synthesized in (a) 7 M LiOH (b) 7 M NaOH and (c) 7 M KOH at 180 °C for 24 h and schematics of morphology shapes from (a1) 7 M LiOH (b1) 7 M NaOH and (c1) KOH.

Similarly, the morphological analysis of the products synthesized for 24 h, as depicted in Figure 3(a), reveals the formation of a mixture resembling a long rectangular shape, contrasting with the observations from the previous synthesis period, as illustrated further in Figure 3(a_1). However, in Figure 3(b), a notable change in shape is observed, resembling a cubic box mixed with rectangular bars, as depicted more clearly in the scheme represented in Figure 3(b_1). Figure 3(c) shows a product with an unchanged shape, yet exhibiting clearer particle edges and corners, as clearly presented in Figure 3(c_1). The results from the SEM suggest that the synthesized product was calcium titanate, consistent with the findings of Li *et al.* [27] and Ernawati *et al.* [9]. The morphology of all products exhibits various shapes and sizes, influenced by different alkali hydroxides and synthesis times. Specifically, the morphology observed in the synthesized product

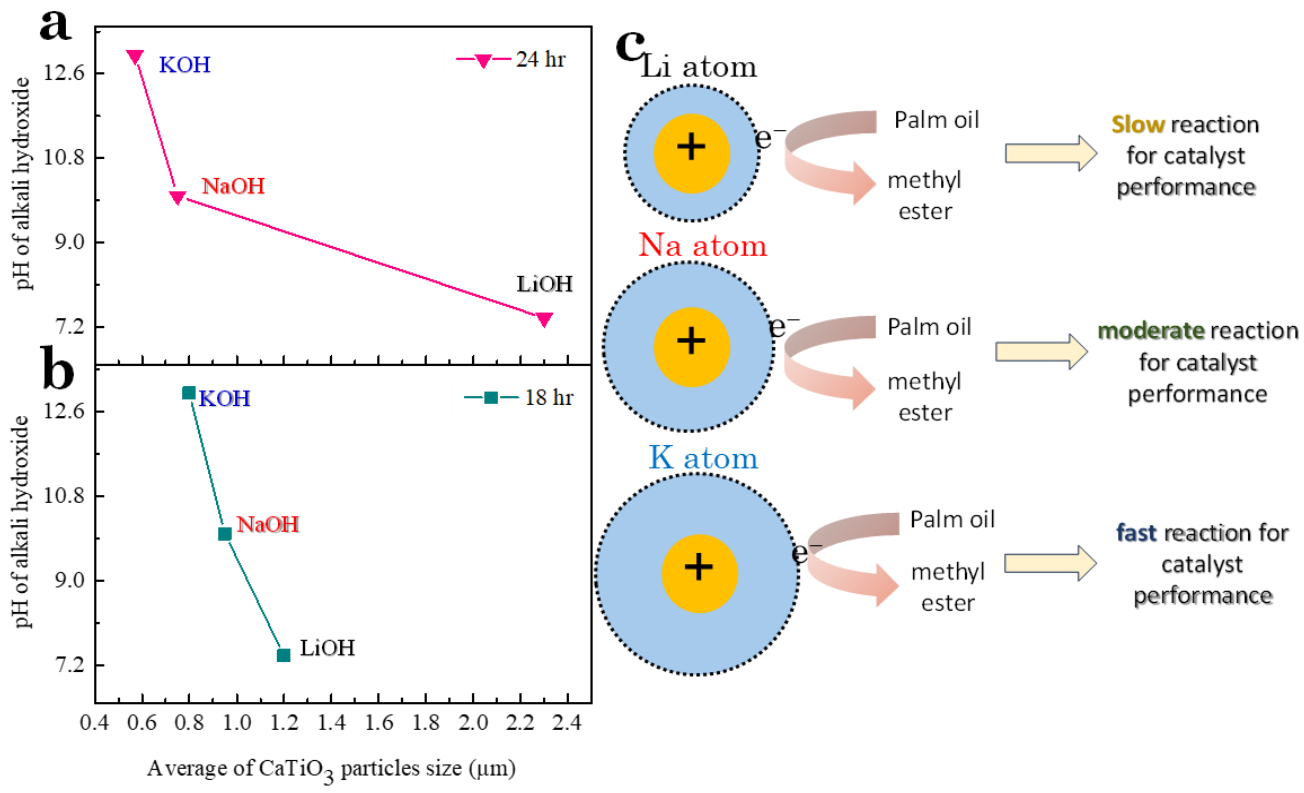

Figure 4. The plot of pH of alkali hydroxide and morphology size from hydrothermal synthesize (a) 18 h, (b) 24 h and (c) the relationship of the atomics size of alkali hydroxide and reactivity of the catalyst.

Copyright © 2024, ISSN 1978-2993

after 24 h of synthesis represents a distinct morphology reminiscent of clear single crystals. This observation corresponds with the FTIR results shown in Figure 1, which indicate strong vibrational modes of Ca–Ti–O in the synthesized products.

To better understand how the type of alkali hydroxide used, and the duration of the hydrothermal process affect the size and morphology of the $CaTiO_3$ crystals, the data is presented in Figures 4(a) and 4(b). Figure 4(a) shows a graph that plots the pH of various alkali

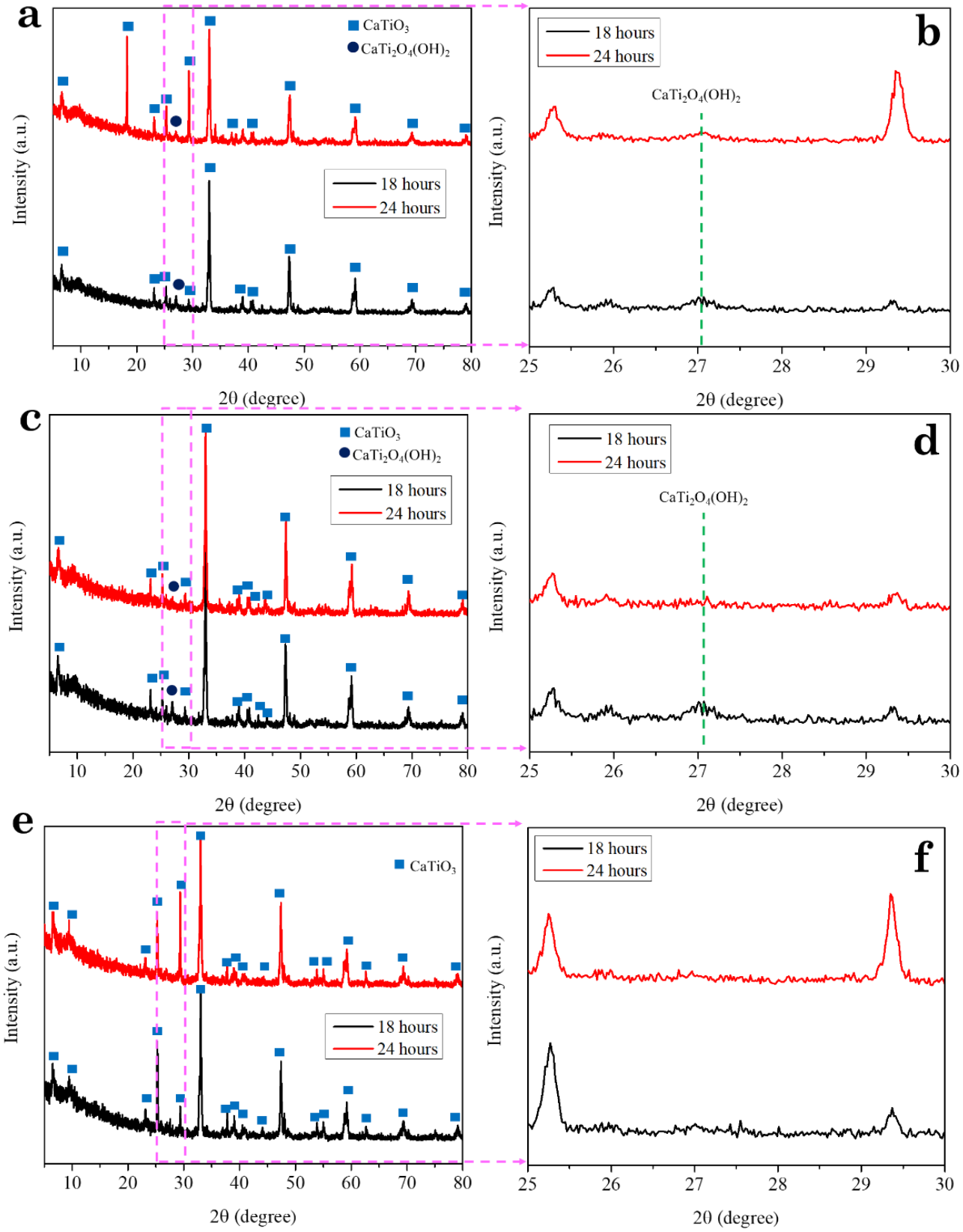

Figure 5. The XRD diffraction of calcium titanate in 7 M from (a) LiOH, (b) NaOH and (c) KOH.

Copyright © 2024, ISSN 1978-2993

hydroxide solutions against the morphology size of $CaTiO_3$ crystals synthesized under hydrothermal conditions for 24 h. The data from this plot demonstrates that an increase in pH correlates with a decrease in the morphology size of the $CaTiO_3$. Additionally, the results indicate that, for the 24 h hydrothermal synthesis, the crystal size of the $CaTiO_3$ product synthesized using LiOH is notably larger compared to those produced with NaOH and KOH about 1.2, 0.9 and 0.8 μm, respectively. This difference is attributed to the presence of moisture and residue during crystal formation, which affects the final morphology of the $CaTiO_3$ product.

In Figure 4(b), the morphology size of $CaTiO_3$ observed at 18 h of hydrothermal treatment shows a trend similar trend to that seen at 24 h, but with a notable increase in the size of the crystals and not closer alignment of sizes across different alkali hydroxides. This observation suggests that extending the hydrothermal treatment time allows for continued crystal growth, resulting in larger crystals and reducing the variability in size among samples synthesized with different alkali hydroxides. This size enhancement can be attributed to the combined effects of increased pH values and prolonged hydrothermal treatment time, which together promote more effective crystallization processes. As a result, the average crystal sizes are 2.3 μm for LiOH, 0.8 μm for NaOH, and 0.7 μm for KOH, reflecting how different alkali hydroxides influence the final crystal size under these conditions.

The effects of different types of alkali hydroxides on the size of the $CaTiO_3$ crystals can be attributed to variations in atomic size and pH values. A high pH value facilitates the formation of metal ions and hydroxide anions more quickly, which in turn affects the crystallization process. Additionally, the rates at which different alkali hydroxides ionize are influenced by the atomic sizes of Li, Na, and K. Alkali hydroxides with larger atomic radii, such as KOH, can lose electrons from their valence shell more easily, which enhances their catalytic performance. This phenomenon is illustrated in Figure 4(c), where the varying effectiveness of different alkali hydroxides as catalysts is shown to correlate with their atomic radii and ionization rates [28].

From the XRD pattern of calcium titanate at 7 M concentration of LiOH it is found that the hydrothermal process at 24 h will give a higher purity phase $CaTiO_3$ product than at 18 h as shown in Figure 5(a). However, when the 2θ range is increased to 25°-30° in Figure 5(b), a diffraction peak corresponding to the by-product phase $CaTi_2O_4(OH)_2$ at 27.05° is observed in samples from both 18 h and 24 h. This observation indicates that LiOH is not suitable for the effective growth formation of $CaTiO_3$. The same as calcium titanate synthesized from NaOH at the hydrothermal process at 24 h will give the $CaTiO_3$ phase with higher purity than the 18 h found phase of $CaTi_2O_4(OH)_2$ as shown in Figure 5(c). But in the case of the KOH based substrate in Figure. Figure 5(d) shows that in the 2θ range of 25°-30°, the diffraction pattern reveals the presence of the by-product phase $CaTi_2O_4(OH)_2$ at 18 h of hydrothermal treatment, which is absent by 24 h. This observation indicates that the by-product phase forms during the initial stages of the synthesis but is no longer present at the extended hydrothermal time, possibly due to the continued reaction or transformation processes.

In Figure 5(d), it is found that regardless of the hydrothermal process at 18 or 24 h, only one phase of $CaTiO_3$ is found. In the 2θ range of 25°-30°, as shown in Figure 5(d), the diffraction pattern does not exhibit the presence of the by-product phase $CaTi_2O_4(OH)_2$ at either 18 h or 24 h of hydrothermal treatment. Due to KOH is strong base is better than LiOH and NaOH which makes it easier to react and is better than other bases. From the XRD results, it is evident that increasing the hydrothermal synthesis time leads to higher purity in the product. Furthermore, the XRD results are complemented by SEM in Figure 3(a_1, b_1, c_1) observations, indicating an increase in the presence of single crystals of $CaTiO_3$.

When considering the heating time required for the hydrothermal process it is observed that as the reaction duration increases the resulting product exhibits higher purity. The crystallinity approaching the nanoscale directly influences the functionality of the catalyst. Based on the results obtained from FTIR, SEM, and XRD analyses, the $CaTiO_3$ synthesized under 7 M alkali hydroxide with heating times of 18 and 24 h continued to be utilized as biodiesel catalysts.

3.2 Transesterification Reaction by $CaTiO_3$ as Biodiesel Catalysts

The biodiesel product was prepared through a transesterification reaction utilizing palm oil heated at 65-70 °C for 3 h. $CaTiO_3$ synthesized via the hydrothermal method for 18 and 24 h under 7 M concentrations of LiOH, NaOH, and KOH was employed as the biodiesel catalyst. The methyl ester of biodiesel was characterized by FTIR. In Figure 6(a), FTIR spectrum was shown the band at 1743 cm^{-1} assigned to the C=O stretch of the ester is observed in both palm oil and biodiesel produced using KOH as a catalyst. In the 1500-100 cm^{-1} range in Figure 6(b) shows that the FTIR spectra reveal the $-CH_3$ bending vibrations at 1461 cm^{-1} and 1377 cm^{-1}, C–O stretching vibrations at 1377 cm^{-1} and 1117 cm^{-1}, and a broad peak at 1243 cm^{-1} for the $O-CH_3$ group across all palm oil and biodiesel samples.

Copyright © 2024, ISSN 1978-2993

Figure 6(c) shows the FTIR spectra of biodiesel produced from $CaTiO_3$ under 18 h of hydrothermal treatment. The spectrum reveals that the catalysts LiOH and NaOH primarily exhibit a broad peak and only a characteristic peak for $-CH_3$ at 1462 cm^{-1}. When the vibrational range is magnified to 1500-100 cm^{-1} in Figure 6(d), it is evident that the biodiesel products from both LiOH and KOH show a band for $-CH_3$. However, the biodiesel product from $CaTiO_3$ under KOH also displays additional peaks at 1377 cm^{-1} and 1118 cm^{-1} corresponding to C–O stretching vibrations. This indicates that the biodiesel produced from $CaTiO_3$ under KOH has a more complex structure compared to those produced with LiOH and NaOH. Overall, the

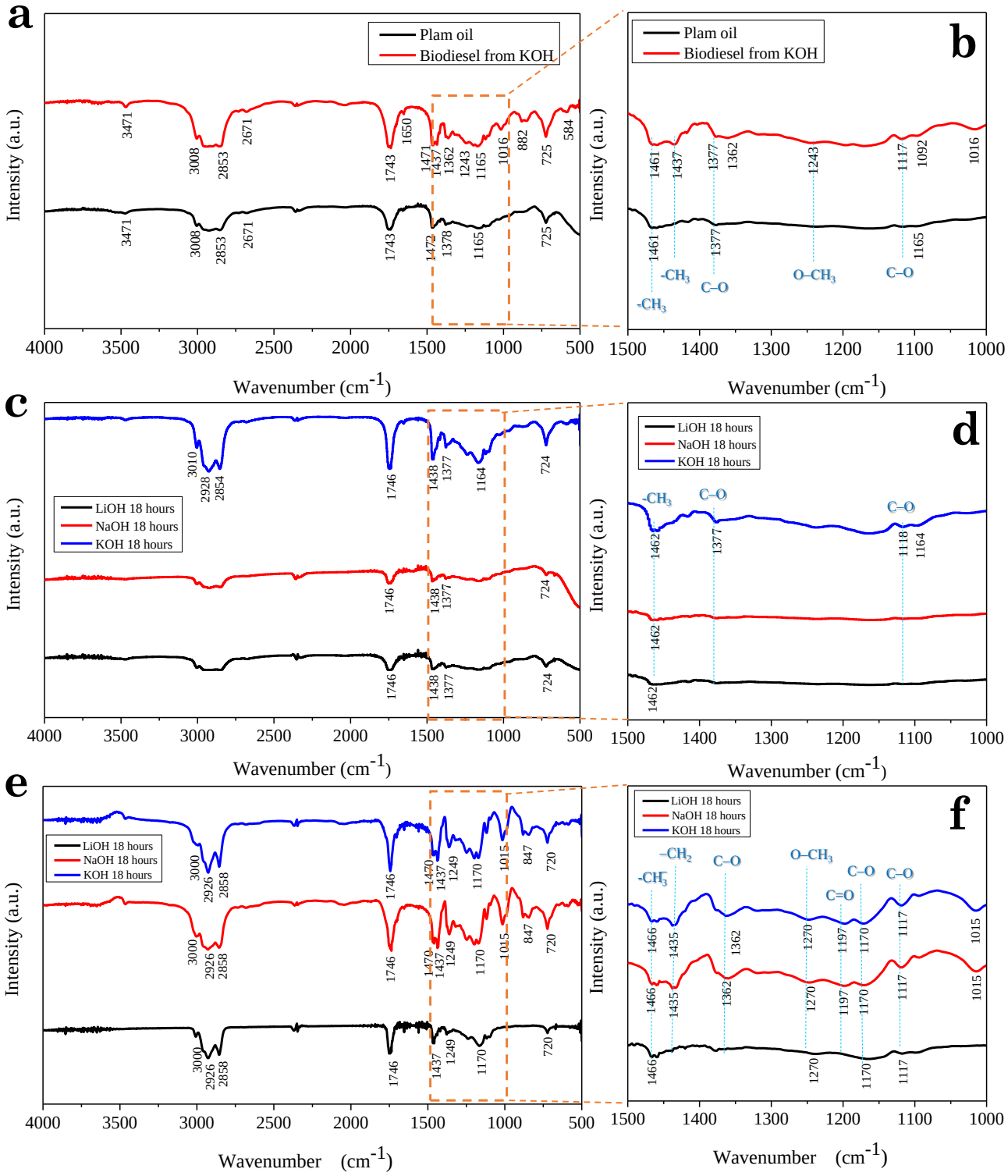

Figure 6. The FTIR spectrum of (a) palm oil and biodiesel by using KOH as catalyst, (b) oil products using $CaTiO_3$ catalysts under 7 M of alkali hydroxide at 18 h and (c) oil products using $CaTiO_3$ catalysts under 7 M of alkali hydroxide at 24 h.

Copyright © 2024, ISSN 1978-2993

performance of the catalysts for transforming palm oil to methyl ester is relatively low for the 18 h hydrothermal synthesis process.

Figure 6(e) shows the FTIR spectra of biodiesel produced from the catalyst under 24 h of hydrothermal synthesis. Compared to the 18 h synthesis, the 24 h spectra exhibit more distinct characteristic peaks, indicating a richer profile of the biodiesel product. However, upon closer examination, it is observed that the spectrum of biodiesel from the $CaTiO_3$ under LiOH catalyst shows a broader peak compared to the spectra from $CaTiO_3$ under NaOH and KOH. This indicates that the biodiesel from $CaTiO_3$ under LiOH has a more complex structure or different molecular interactions. When the spectra are magnified in the 1500-1000 cm^{-1} range, as shown in Figure 6(f), the characteristic features of the biodiesel production become more apparent and allow for a clearer comparison of the effects of different catalysts.

The FTIR spectra of biodiesel from the catalyst under LiOH conditions after 24 h of hydrothermal synthesis show distinct vibrational peaks at 1466 cm^{-1} for $-CH_3$, 1170 cm^{-1} and 1117 cm^{-1} for C–O, and 1270 cm^{-1} for $O-CH_3$. In contrast, the biodiesel products from catalysts under NaOH and KOH conditions exhibit additional vibrational features including a peak at 1466 cm^{-1} for $-CH_3$, 1435 cm^{-1} for $-CH_2$, 1362 cm^{-1}, 1170 cm^{-1}, and 1117 cm^{-1} for C–O, 1197 cm^{-1} for C=O, and 1270 cm^{-1} for $O-CH_3$. The presence of these additional peaks in the FTIR spectra indicates that the biodiesel produced using NaOH and KOH catalysts has a more complex composition compared to that produced with LiOH. Furthermore, the comparison of these spectra with those from the 18-h hydrothermal synthesis process demonstrates that the 24 h synthesis generally results in higher catalyst performance for the production of biodiesel, as evidenced by the more diverse range of vibrational modes observed in the spectra.

Table 1 presents the physical and chemical properties of the biodiesel products obtained using $CaTiO_3$ as a catalyst under various conditions. Specifically, the biodiesel yield using $CaTiO_3$ with a 7 M LiOH solution was approximately 87% for an 18 h reaction time and 95% for a 24 h reaction time. Despite these high yield percentages, the GC-MS data failed to detect any %FAME which indicates that the $CaTiO_3$ catalyst under LiOH conditions was not effective for the transesterification reaction and viscosity are 34.67 cSt and 34.98 cSt. This suggests that while the reaction conditions resulted in a high volume of biodiesel, the quality or composition of the biodiesel did not meet the criteria for successful transesterification as determined by GC-MS analysis.

The results for the NaOH-catalyzed biodiesel production under 18 h and 24 h are shown as follows the percentage of biodiesel yield was 70% for 18 h and 78% for 24 h, with corresponding viscosities of 34.98 cSt and 5.14 cSt, respectively. Although the %FAME was not detected at 18 h, it was found to be 63.67% at 24 h. These results suggest that the longer reaction time improves the %FAME content in the biodiesel. In comparison, the high viscosity observed for the biodiesel produced using $CaTiO_3$ under both LiOH and NaOH conditions indicates that the transesterification reaction was not successful for biodiesel production, as evidenced by the inadequate %FAME formation and the high viscosity of the final product.

Under hydrothermal conditions, the KOH-catalyst demonstrated biodiesel yields of 90% after 18 h and 93% after 24 h. While %FAME could not be detected in the biodiesel produced after 18 h, the 24 h reaction resulted in a high %FAME content of 90.02%. It corresponds with viscosities of 32.61 cSt and 4.98 cSt for the 18 h and 24 h reactions, respectively. This significant increase in %FAME and the low viscosity of the biodiesel product after 24 h highlight the effectiveness of $CaTiO_3$ as a catalyst for the transesterification reaction when used under optimal hydrothermal conditions. Thus, the results indicate that $CaTiO_3$ under these conditions is a suitable and efficient catalyst for biodiesel production.

Table 1. The viscosity, the yield of biodiesel and % fatty acid methyl ester (FAME) of oil product by $CaTiO_3$ as biodiesel catalyst.

$CaTiO_3$ under 7 M of alkali hydroxide	Heating time of hydrothermal method (h)	The yield of biodiesel (%)	Viscosity of biodiesel (cSt)	% FAME
LiOH	18	87	34.67	-
NaOH	18	70	34.98	-
KOH	18	90	32.61	-
LiOH	24	95	33.97	-
NaOH	24	78	5.14	63.67
KOH	24	93	4.98	90.02

Copyright © 2024, ISSN 1978-2993

The $CaTiO_3$ catalyst proves to be an effective catalyst for the transesterification reaction under KOH conditions for 24 h. This effectiveness is comparable to that of traditional strong bases such as NaOH and KOH due to the high basicity of KOH, which facilitates the transesterification process. However, a significant advantage of using $CaTiO_3$ is its potential for reuse, which reduces waste compared to traditional base catalysts.

The reaction steps and overall process for using $CaTiO_3$ as a catalyst are illustrated in Figures 7(a) and 7(b), demonstrating both the efficiency of the transesterification reaction and the sustainability benefits of the $CaTiO_3$ catalyst. Table 2 presents a comparison of the catalytic performance of $CaTiO_3$ under KOH conditions for 24 h with that of other catalysts reported in previous studies. This comparison demonstrates that $CaTiO_3$ exhibits high catalytic performance for the transesterification reaction, showing superior or comparable results to other catalysts used for biodiesel production. This finding highlights a significant new development for $CaTiO_3$ as an effective and innovative catalyst for biodiesel synthesis under KOH conditions for 24 h, suggesting its potential for future applications in biodiesel production.

4. Conclusions

In this study, we have demonstrated the pivotal role of 7 M concentrations of NaOH and KOH in achieving optimal synthesis conditions for calcium titanate via the hydrothermal method at 180°C for 24 hours. The successful formation of $CaTiO_3$ was confirmed through rigorous analysis using FTIR and XRD, referencing JCPDS No. 42-0423. SEM analysis further elucidated the distinct cube-like morphology of calcium titanate, suggesting its potential suitability for a wide range of catalytic applications. Notably, our investigation revealed a significant difference in the percentage yields of fatty acid methyl ester obtained using calcium titanate synthesized with NaOH (63.67%) compared to KOH (90.02%), underscoring the critical role of the alkali hydroxide choice in optimizing catalyst performance.

These findings contribute to the growing body of knowledge on calcium titanate synthesis and its application in biodiesel production. The ability to tailor synthesis conditions to achieve desired catalytic properties opens avenues for further research into optimizing biodiesel production processes. Future studies could explore the underlying mechanisms influencing catalyst performance and investigate additional synthesis parameters to enhance catalytic activity and selectivity.

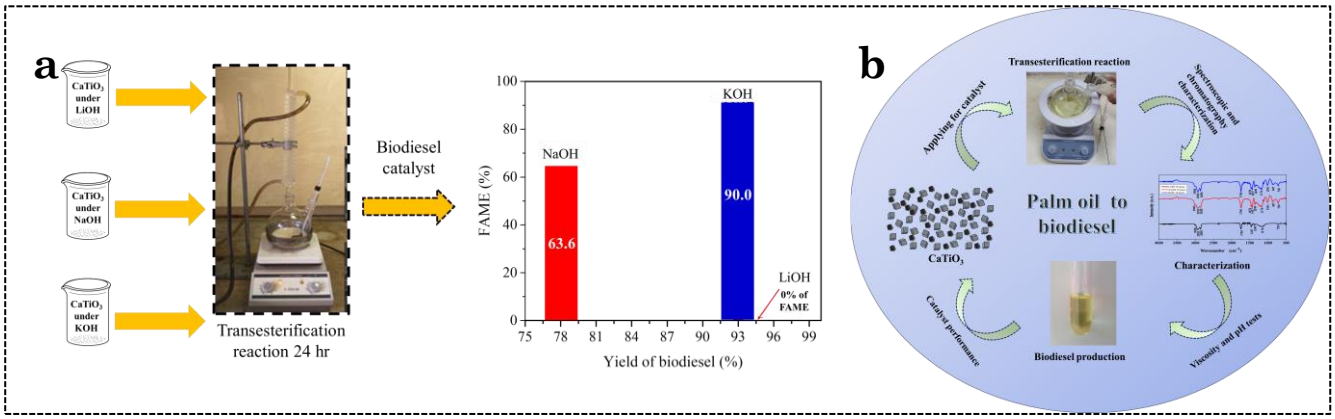

Figure 7. (a) The percentage of FAME by $CaTiO_3$ as biodiesel catalyst. (b) The flow diagram for biodiesel production from palm oil by using $CaTiO_3$ as a catalyst.

Table 2. Comparison of the percentage of FAME of other materials with previous reports.

Catalyst	Synthesize method	% FAME	Type of reaction	Reference
$Na_2Ti_3O_7$	hydrothermal	69.05	transesterification	[7]
K/TiHT	hydrothermal	65.0	transesterification	[30]
TS-0	sol–gel	30.0	transesterification	[31]
*$CaTiO_3$	sol-gel-hydrothermal	80.0	transesterification	[32]
*TNT	hydrothermal	83.5	transesterification	[33]
$CaTiO_3$	hydrothermal	90.0	transesterification	This work

*nano tube

Copyright © 2024, ISSN 1978-2993

Overall, our results highlight the importance of careful selection and optimization of synthesis parameters in achieving efficient catalysts for biodiesel production. By advancing our understanding of calcium titanate synthesis and its catalytic properties, this study offers valuable insights for the development of sustainable and efficient processes in the biodiesel industry.

Acknowledgment

The authors would like to thank the following institution for its financial support: Faculty of Science, Maejo University.

CRediT Author Statement

Conceptualization, writing-review, writing-original draft preparation, writing-editing, visualization; Ratchadaporn Puntharod.; methodology, Kittikarnkorn Onsomsuay.; software, writing-review and editing, Jaturon Kumchompoo.; conceptualization and formal analysis, Pusit Pookmanee.

References

[1] Ji, H., Ni, J., Zhao, D., Liu, W. (2022). Application of titanate nanotubes for photocatalytic decontamination in water: challenges and prospects. *Environmental Science & Technology*, 2, 1015-1038. DOI: 10.1021/acsestengg.1c00451.

[2] Ahmadipour, M., Ain, M.F, Ahmad, Z.A. (2016). A short review on copper calcium titanate (CCTO) electro ceramic: synthesis, dielectric properties, film deposition, and sensing application. *Nano-Micro Letters*, 8, 291-311. DOI: 10.1007/s40820-016-0089-1.

[3] Yan, H., Zhang, D. Qilu., Duon, X., Sheng, X. (2021). A review of spinel lithium titanate ($Li_4Ti_5O_{12}$) as electrode material for advanced energy storage devices. *Ceramic International*, 47, 5870-5895. DOI: 10.1016/j.ceramint.2020.10.241.

[4] Lebedev, A.I. (2009). Ab initio calculations of phonon spectra in $ATiO_3$ perovskite crystals (A= Ca, Sr, Ba, Ra, Cd, Zn, Mg, Ge, Sn, Pb). *Physics of the Solid State*, 51, 362–372. DOI: 0.1134/S1063783409020279.

[5] Hernández-Hipólito, P., García-Castillejos, M., Martínez-Klimova, E., Juárez-Flores, N., Gómez-Cortés, A., Klimova, T.E. (2014). Biodiesel production with nanotubular sodium titanate as a catalyst. *Catalysis Today*, 220-222, 4-11. DOI: 10.1016/j.cattod.2013.09.003.

[6] Sahani, S., Roy, T., Sharma, Y.C. (2020). Studies on fast and green biodiesel production from an indigenous nonedible indian feedstock using single phase strontium titanate catalyst. *Energy Conversion and Management*, 203, 112180. DOI: 10.1016/j.enconman.2019.112180.

[7] Machorro, López J.J., Lázaro, A.L., Rodriguez-Valadez, F.J., Espejel-Ayala, F. (2020). Synthesis of sodium titanate catalysts using a factorial design for biodiesel production. *Environmental Progress Sustainable Energy*, 40, 13475. DOI: 10.1002/ep.13475.

[8] Ahmad, K., Kumar, P., Mobin, S.M. (2020). Hydrothermally grown novel pyramids of $CaTiO_3$ perovskite as efficient electrode modifiers for sensing applications. *Materials Advances*, 1, 2003-2009. DOI: 10.1039/D0MA00303D.

[9] Ernawati, L., Yusariarta, A.W., Laksono, A.D., Wahtuono, R. A., Widiyandari, H., Rebeka, R., Sitompul, V. (2021). Kinetic studies of methylene blue degradation using $CaTiO_3$ photocatalyst from chicken eggshells. *Journal of Physics: Conference Series*, 1726, 012017. DOI: 10.1088/1742-6596/1726/1/012017.

[10] Yahya, N.Y., Ngadi, N., Wong, S., Hassan, O. (2018). Transesterification of used cooking oil (UCO) catalyzed by mesoporous calcium titanate: kinetic and thermodynamic studies. *Energy Conversion and Management*, 164, 210-218. DOI: 10.1016/j.enconman.2018.03.011.

[11] Ali, M.A., Al-Hydary, I.A., Al-Hattab, T.A. (2017). Nano-magnetic catalyst CaO-Fe_3O_4 for biodiesel production from date palm seed oil. *Bulletin of Chemical Reaction Engineering & Catalysis*, 12, 460-468. DOI: 10.9767/bcrec.12.3.923.460-468.

[12] Yahya, N.Y., Ngadi, N., Jusoh, M., Halim, N.A.A. (2016). Characterization and parametric study of mesoporous calcium titanate catalyst for transesterification of waste cooking oil into biodiesel. *Energy Conversion and Management*, 129, 275-283. DOI: 10.1016/j.enconman.2016.10.037.

[13] Chozhavendhan, S., Pradhap, Singh M.V., Fransila, B., Kumar, R.P., Karthiga Devi, G. (2020). A review on influencing parameters of biodiesel production and purification processes. *Current Research in Green and Sustainable Chemistry*, 1(2), 1-6. DOI: 10.1016/j.crgsc.2020.04.002.

[14] Yatish, K.V., Lalithamba, H.S., Suresh, R., Latha, H.K.E. (2020). Ochrocarpus longifolius assisted green synthesis of $CaTiO_3$ nanoparticles for biodiesel production and its kinetic study. *Renewable Energy*, 147, 310-321. DOI: 10.1016/j.renene.2019.08.139.

[15] Kawashima, A., Matsubara, K., Honda, K, (2008). Development of heterogeneous base catalysts for biodiesel production. *Bioresource Technology*, 99, 3439–3443. DOI: 10.1016/j.biortech.2007.08.009.

[16] Lanfredi, S., Matos, J da Silva S.R., Djurado, E., Sadouki, A.S., Chouaih, A., Poon, P.S., González, E.R.P Nobre M.A.L. (2020). K- and Cu-doped $CaTiO_3$-based nanostructured hollow spheres as alternative catalysts to produce fatty acid ethyl esters as potential biodiesel. *Applied Catalysis B: Environment and Energy*, 2721, 18986. DOI: 1016/j.apcatb.2020.118986.

Copyright © 2024, ISSN 1978-2993

[17] Istadi, I., Mabruro, U., Kalimantini, B.A., Buchori, L., Anggoro, D.D. (2016). Reusability and stability tests of calcium oxide based catalyst (K_2O/CaO-ZnO) for transesterification of soybean oil to biodiesel. *Bulletin of Chemical Reaction Engineering & Catalysis*, 11, 34-39. DOI: 10.9767/bcrec.11.1.413.34-39.

[18] Hadiyanto, H., Lestari, S.P., Widayat, W. (2016). Preparation and characterization of Anadara Granosa shells and $CaCO_3$ as heterogeneous catalyst for biodiesel production. *Bulletin of Chemical Reaction Engineering & Catalysis*, 11, 21-26. DOI: 10.9767/bcrec.11.1.402.21-26.

[19] Dong, W., Song, B., Zhao, G., Han, G. (2015). A simple solvothermal process to synthesize $CaTiO_3$ microspheres and its photocatalytic properties. *Applied Surface Science*, 349, 272-278. DOI: 10.1016/j.apsusc.2015.05.006.

[20] Dong, W., Zhao, G., Bao, Q., Gu, X. (2015). Solvothermal preparation of $CaTiO_3$ prism and $CaTi_2O_4(OH)_2$ nanosheet by a facile surfactant-free method. *Material Science*, 21, 583-585. DOI: 10.5755/j01.ms.21.4.9697.

[21] Kumchompoo, J., Puntharod, R., (2022). Synthesis and characterization of lithium silicate and potassium silicate from rice husk ash by hydrothermal-microwave method and application for biodiesel catalyst. *Suranaree Journal of Science and Technology*, 29(3), 010137.

[22] Velmurugan, A., Warrier, A.R. (2022). Production of biodiesel from waste cooking oil using mesoporous MgO-SnO_2 nanocomposite. *Journal of Engineering and Applied Science*, 69, 1-22. DOI: 10.1186/s44147-022-00143-y.

[23] Rahman, M.A., Aziz, M.A., Al-khulaidi, R.A., Sakib, N., Islam, M. (2017). Biodiesel production from microalgae Spirulina maxima by two step process: Optimization of process variable. *Journal of Radiation Research and Applied Sciences*, 10, 140-147. DOI: 10.1016/j.jrras.2017.02.004.

[24] Salam, K.A., Velasques-Orta, S.B., Harvey, A.P. (2017). Effect of soaking pre-treatment on reactive extraction/in situ transesterification of nannochloropsis occulata for biodiesel production. *Journal of Sustainable Bioenergy Systems*, 7, 149-164. DOI: 10.4236/jsbs.2017.74011.

[25] Chozhavendhan, S., Pradhap, Singh M.V., Fransila, B., Kumar, R.P., Karthiga, Devi G. (2020). A review on influencing parameters of biodiesel production and purification processes. *Current Research in Green and Sustainable Chemistry*, 1(2), 1-6. DOI: 10.1016/j.crgsc.2020.04.002.

[26] Han, C., Liu, J., Yang, W., Wu, Q., Yang, H., Xue, X. (2016). Enhancement of photocatalytic activity of $CaTiO_3$ through HNO_3 acidification. *Journal of Photochemistry and Photobiology A: Chemistry*, 322-323, 1-9. DOI: 10.1016/j.jphotochem.2016.02.012.

[27] Li, S., Zhang, J., Jamil, S., Cai, Q., Zang, S., (2018). Conversion of eggshells into calcium titanate cuboid and its adsorption properties. *Research on Chemical Intermediates*. 44. 3933-3946. DOI: 10.1007/s11164-018-3332-1.

[28] Hindryawati, N., Maniam, G.-P., Karim, MD.-R., Chong, K-F. (2014). Transesterification of used cooking oil over alkali metal (Li, Na, K) supported rice husk silica as potential solid base catalyst. *Engineering Science and Technology, an International Journal*, 17, 95-103. DOI: 10.1016/j.jestch.2014.04.002.

[29] Muhamuni, N.N., Adewuyi, Y.G. (2009). Fourier transform infrared spectroscopy (FTIR) method to monitor soy biodiesel and soybean oil in transesterification reactions, petrodiesel–biodiesel blends, and blend adulteration with soy oil. *Energy Fuels*, 23, 3773-3782. DOI: 10.1021/ef900130m.

[30] Salinas, D., Araya, P., Guerrero, S. (2012). Study of potassium-supported TiO_2 catalysts for the production of biodiesel. *Applied Catalysis B: Environment and Energy*, 117-118, 260-267. DOI: 10.1016/j.apcatb.2012.01.016.

[31] Marciniuk, L.L., Hammer, P., Pastore, H.O., Schuchardt, U., Cardoso, D., (2014). Sodium titanate as basic catalyst in transesterification reactions. *Fuel*, 118, 48-54. DOI: 10.1016/j.fuel.2013.10.036.

[32] Yahya, N.Y., Ngadi, N., Jusoh, M., Halim, N.A.A. (2016). Characterization and parametric study of mesoporous calcium titanate catalyst for transesterification of waste cooking oil into biodiesel. *Energy Conversion and Management*, 129, 275-283. DOI: 10.1016/j.enconman.2016.10.037.

[33] Nady, D., Zaki, A.H., Raslan, M., Hozayen, W. (2020). Enhancement of microbial lipase activity via immobilization over sodium titanate nanotubes for fatty acid methyl esters production. *International Journal of Biological Macromolecules*, 146, 1169-1179. DOI: 10.1016/j.ijbiomac.2019.09.240.

Copyright © 2024, ISSN 1978-2993